Proceedings of the 3rd International Conference on Materials Chemistry and Environmental Engineering (CONF-MCEE 2023), Part II
DOI: 10.54254/2755-2721/7/20230545

Triangulated cylindrical origami: Design and experimental investigation

Zhenhao Xue

Darlington School, Rome, GA 30161, United States

zxue@darlingtonschool.org

Abstract. Origami-based mechanical metamaterials have emerged in multiple technologies, such as vehicle and wearable equipment industries, thanks to their appealing mechanical performances. The excellent energy absorption capability, multi-stability, tunable stiffness, and stretchability of origami metamaterials enable them to adapt easily to different working requirements. Among all the origami metamaterial structures, triangulated cylinder origami (TCO) has been one of the most useful ones. In this research paper, a parametric study based on experiments and data analysis is performed to explore the effect of design parameters on the strain and strength of the TCOs. It was revealed that while the relative orientation of units in each column has no significant impact on the mechanical properties of the TCOs, the number of units in each column, *n*, plays an important role. It was discovered that a hexagon TCO with *n* of 6 offers higher strain and strength compared to an octagon TCO with *n* of 8. This study aims to pave the road for later optimization of TCOs for building materials and foldable structures applications.

Keywords: Metamaterials, Origami, Triangulated Cylinder, Mechanical Performance.

1. Introduction

The growing demand for materials with enhanced mechanical properties has led to the development of various technologies that aim to improve specific mechanical characteristics by altering the microstructure of the materials. Mechanical metamaterials are specifically engineered materials with unconventional mechanical properties. Origami, a traditional Japanese art known for its techniques of folding 2D patterns into 3D structures, provides new ways to manipulate the structures and pave the way for a kind of promising mechanical metamaterials, origami metamaterials [1]. With their outstanding mechanical performances, origami-based mechanical metamaterials have been applied in many fields, including flexible electronics [2-5], medical devices [6, 7], and robotics [8-12].

Diverse folding patterns of origami metamaterials give them different mechanical performances suitable for various scenarios. Most origami patterns that are used today are rigid-foldable, Kresling/Yoshimura, and curved patterns. Rigid-foldable patterns involve folding and unfolding 2D origami patterns into 3D origami structures without deforming them. Among rigid-foldable patterns, there are two sub-species based on their transformation mode, one degree of freedom (DOF) type and multi-DOF type. The number of creases determines the DOF of origami patterns at each vertex [2]. One-DOF-type origami patterns have four creases per vertex, such as the Miura pattern. Miura patterned 2D panels have unique mechanical properties and multiple layers which can be assembled to gain a better

DOI: 10.54254/2755-2721/7/20230545

performance [13]. Therefore, it has been applied in many areas, such as energy harvesting devices [14] and shape recovery materials [15]. The multi-DOF type origami has more than four creases per vertex, such as Ron Resch [16], waterbomb origamis [17], square-twist [18], Kresling tube [19], and hypar origami [20].

Energy absorption (EA) capability is an essential property of origami metamaterials. The EA can be significantly enhanced by manipulating the folding pattern of origami metamaterial. Xiang *et al.* proposed a thin-walled origami tube with a higher EA capacity, lower peak force, and lower force fluctuation, which are ideal properties of EA structures [21]. One of the typical applications is the crash box of vehicles. An experimental test was performed by Boreanaz *et al.* on origami-structured crash boxes, and a better EA performance was observed [22].

The multi-stability of origami metamaterials is another attractive mechanical property of origami metamaterials. Compared to one DOF-type origami pattern, multi-DOF origami patterns have remarkable multi-stability. However, due to their irregular geometry, the difference in deformation mode, and the multi-stable energy landscape between each unit cell, it is challenging to tesselate many of those multi-DOF origami patterns and predict their behaviors. To obtain better multi-stable origami patterns, many researchers optimized those patterns by collaborating knowledge of other areas. Liu *et al.* proposed a novel multi-stable origami pattern imitating the body shape of shrimps, making it easy to tessellate the pattern [23]. Overvelde *et al.* also created a periodic structure consisting of extruded cubes which each have three DOF. The fabricated 3D structure can be deformed into numerous shapes with an embedded actuation mechanism [24].

In addition to multi-stability, another outstanding mechanical property of origami metamaterials is tunable stiffness. Plenty of stiffness-tunable structures were developed based on triangulated cylinder patterns, waterbomb patterns, and curved origami patterns [17, 25-28]. A deployable and selectively collapsible system with triangulated cylinder origami (TCO) pattern was proposed by Zhai *et al.* This structure has different stiffness at different states under different loading paths [25]. Mukhopadhyay *et al.* developed an origami metamaterial with programmable stiffness based on a water bomber origami pattern [26]. Feng *et al.* discovered that the continuous twisting motion of the water bomb pattern-based origami tube enhances its stiffness [17]. Wen *et al.* proposed a zigzag-base stacked-origami metamaterial (ZBSO) that manipulates stiffness by altering the curvature of the creases. They also revealed that this structure's self-locking mechanism and asymmetrical stiffness distribution contribute to its multi-stage stiffness [27]. To widen the design space of origami metamaterial with tunable mechanical properties, some efforts were made to open the gateway from flat-foldable patterns to nonflat-foldable patterns. Fang *et al.* found that the self-locking mechanism ensures nonflat-foldable patterns have larger geometry design space and can be manipulated to a broader range of foldability and relative density [28].

Besides, the coefficient of thermal expansion is also a parameter that researchers are eager to govern. Boatti *et al.* reported that the transformation of the Miura-origami structure could change the coefficient of thermal expansion. In their research, configurations with different arrangements of single and bilayer of Miura-origami, stiffness of the creases, and geometric parameters were tested and showed a variety of coefficients of thermal expansion [29]. In addition, by altering the geometric parameters of graphene origami material, various adatom types, density, and mechanical strains are achievable [30]. The tunability of these properties makes origami metamaterial a great candidate for next-generation thermoelectric devices, heat management systems, and flexible nanoelectronics [30].

Various origami patterns and their unique properties have been studied so far, but there are still undiscovered relationships between crucial design parameters and the mechanical properties of origami metamaterials. Hence, we here focus on the parametric study of the TCO, which can develop coupled dynamics of axial and rotational motions during folding and unfolding. Furthermore, the impact of the angle of each unit, the number of units in a row, and the direction of each row on the mechanical performance of TCO are theoretically and experimentally investigated.

DOI: 10.54254/2755-2721/7/20230545

2. Design

Figure 1 (a) shows the 2D pattern (flat sheet) of a TCO with a length of B and width of A, which consists of repeating triangular unit cells. The TCO is characterized by valley crease lines (orange) and mountain crease lines (blue) in figure 1(a). Two adjacent unit cells are illustrated in figure 1(b). A single unit is characterized by the length of one side, b, the height of the unit, a, and the angle between the valley crease line and horizontal black line, α.

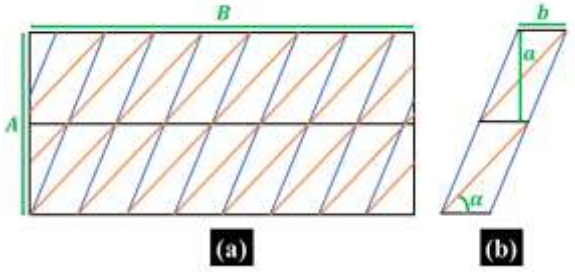

Figure 1. (a) 2D pattern of a TCO and (b) its two adjacent unit cells. Orange (blue) lies represent valley (mountain) crease lines, respectively.

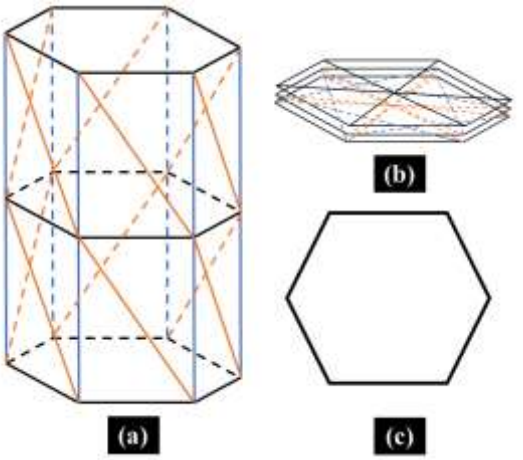

Figure 2. Side views of (a) fully extended and (b) fully folded TCO with two columns and (c) its hexagon shape horizontal cross-section.

Other design parameters may influence the mechanical performance of the TCO. In the scale of the whole cylinder, the number of units in one column, n, and the number of columns, m, are defined as two independent design parameters. When left and right boundaries' triangles are sewed for a closed cylinder, two valley and mountain crease lines intersect at a vertex of the polygon. Therefore, the top and bottom surfaces of the TCO are n-sided polygons with a side length of b. For example, six units in a column result in a TCO with a hexagon shape cross-section, while eight units in a column create a TCO with an octagon shape cross-section. The 3D model of fully extended and folded configurations of a 2-column TCO with a hexagon shape cross section (n=6 and m=2) is shown in figure 2. The mountain, valley, and horizontal folds are presented in blue, orange, and black lines, respectively. In the folded configuration, all folds of the lower column are shown in orange and blue lines, while only the horizontal mountain folds are shown in black lines for the upper column.

In addition, the direction the parallelogram unit of a column slanted towards is defined as the direction of the column. The direction of the columns relative to the adjacent ones, whether the same or different, is defined as another critical design parameter. Among the aforementioned design parameters, several of them are interrelated. For the TCO to be perfectly folded into a perfect polygon, there is a specific rule that regulates a, b, n, and α. For example, the valley and mountain crease lines overlay on the diagonal line connecting the *i* and *iv* vertices and *iv* and *vi* vertices of the hexagon, correspondingly, as shown in figure 3(a). The top view of a hexagon cylinder with only one pair of mountain and valley crease lines is provided. Since the length proportion of each diagonal line to the sideline is fixed in a hexagon, the length of mountain crease lines (m) and length of valley crease lines (v) are calculated to be $\sqrt{3}b$ and $2b$, correspondingly. Thus, being projected to a unit cell, figure 3 (b), the unit cell is proved

DOI: 10.54254/2755-2721/7/20230545

to be a rectangle by Pythagorean theorem. As a result, in the situation of a hexagon TCO, m equals a, and α is 60°. Similarly, as shown in figure 4, for octagon TCO, a equals 1.71b, and α is 45°.

Here, we fabricate, test, and analyze the TCO structures with hexagon and octagon shape cross sections. With the relationships above determined, the key parameters we focus on are the number of units in each column (n) and the relative direction of units in each column. Other vital parameters are controlled to compare the mechanical performance of different TCO structures effectively.

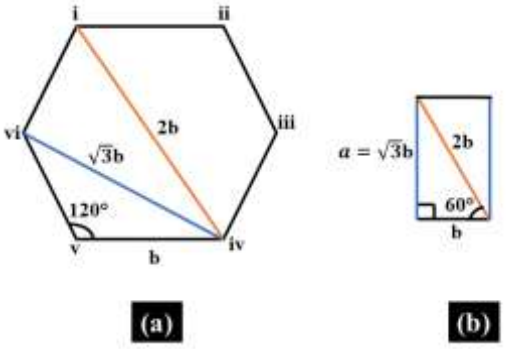

Figure 3. (a) Cross section of a hexagon TCO perfectly folded into a hexagon and (b) its flat unit cell.

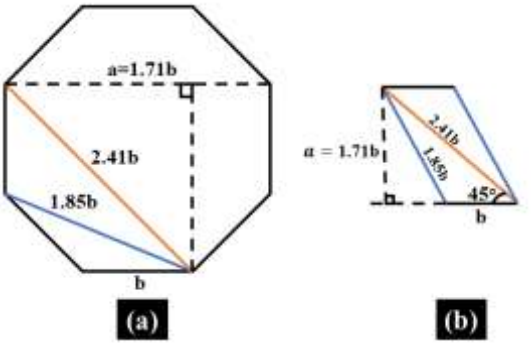

Figure 4. (a) Cross section of an octagon TCO perfectly folded into an octagon and (b) its unit cell.

3. Parametric Study and Fabrication

A parametric study is carried out to investigate the impact of the number of units in a row (n) and the direction of each row (SDO stands for Same Direction Oriented and DDO stands for Different Direction Oriented) on the strain and strength of the TCO. To this end, four different TCO structures can be considered. Table 1 provides the details of each TCO. Structures 1 and 2 with n of 8 and structures 3 and 4 with n of 6 serve as groups to explore the effect of the orientation of the columns (SDO and DDO). Structures 1 and 3 with SDO orientation for columns and structures 2 and 4 with DDO orientation for columns serve as groups to discover the influence of the number of units in a column, n.

Table 1. Number of units in a row (n), angle (α), and direction of each row (SDO or DDO) of the fabricated TCO samples.

Structures Name	**n** and α	The direction of Each Row
1: Octagon-SDO-TCO	Octagon (n=8), $\alpha = 45°$	SDO
2: Octagon-SDO-TCO	Octagon (n=8), $\alpha = 45°$	DDO
3: Hexagon-SDO-TCO	Hexagon (n=6), $\alpha = 60°$	SDO
4: Hexagon-DDO-TCO	Hexagon (n=6), $\alpha = 60°$	DDO

For proof of concept, four different TCO structures are fabricated based on Table 1. The same material (colored A4 paper) is used to fabricate each of the samples. The flat pattern for each fabrication is shown in figure 5. The orange lines represent the valley crease lines, and the blue lines correspond to the mountain crease lines. The width and length of the fabricated TCO structures are listed in Table 2. The width of a single unit is the controlled parameter, which is 3.0 cm for all structures. Following the relationship between n, a, and α, the total width (B) and the total length (A) can be calculated.

After fabrication of the flat patterns for each TCO structure, they are rolled into cylinders with the horizontal folds pointing out, and the stick areas are stuck to the inner wall of the cylinder with double-sided tape. The photographs of fabricated TCO structures are shown in figure 6.

DOI: 10.54254/2755-2721/7/20230545

Table 2. Width and length of the fabricated TCO structures. SA: Sticking Area

	1: Octagon-SDO	2: Octagon-SDO	3: Hexagon-SDO	4: Hexagon-DDO
Width (*B*)	24.0 cm	24.0 cm	18.0 cm	18.0 cm
Length (*A*)	20.4 cm	20.4 cm	20.8 cm	20.8 cm
Width of the SA	1.9 cm	1.9 cm	1.9 cm	1.9 cm
Length of the SA	20.4 cm	20.4 cm	20.8 cm	20.8 cm

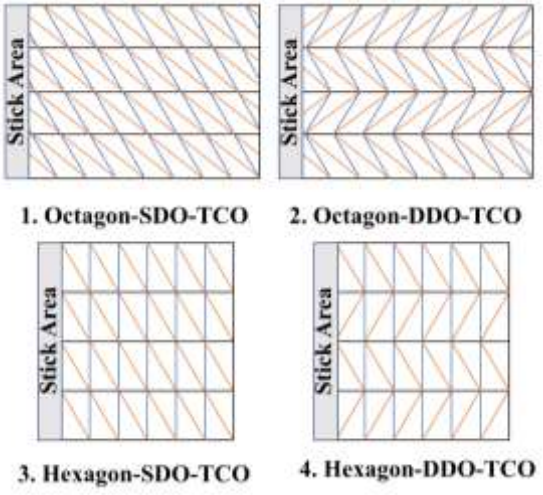

Figure 5. The 2D pattern of the fabricated octagon 2) and hexagon TCO samples.

Figure 6. Photographs of fabricated TCO structures.

Two sets of experiments are designed and executed to evaluate the strain and strength of the TCO samples. In experiment 1, the strain performance of cylinders is evaluated. All the TCOs are fixed on a horizontal surface, completely folded (see figure 7(a)), and their length is recorded (L_0). Next, an upward force is exerted by hand-pulling a string attached to the periphery of the top surface of the TCOs (see figure 7(b)). As the force increases, each column of TCOs is gradually unfolded. The total length of the TCOs is recorded after every unfolding (cumulatively, 1 column unfolded is L_1, cumulatively, two columns unfolded is L_2, *etc*.). By comparing the length of the cylinder in the completely folded state (L_0) with the length of the unfolded state (L_i), where i represents the number of unfolded columns, the strain (ε_i) can be calculated as follow:

$$\varepsilon_i = \frac{L_i - L_0}{L_0}$$

In experiment 2, the strength evaluation is performed. Similar to experiment 1, TCOs are transferred to the completely folded state and fixed on a horizontal surface (see figure 7(a)). The strings are attached to a force sensor which records the force magnitude and transports the data to the computer software, Logger Pro. An upward force is exerted on the force sensor by hands (see figure 7(c)). The force is gradually increased until the TCO is fully stretched to a 4-columns-unfolded state. Strength is defined as the maximum force a TCO structure experiences before unfolding. The TCO structure resists the folded-unfolded transformation till the applied force reaches its maximum. This transformation appears as a valley in the force-time graph. Therefore, the maximum force before each valley was recorded as the strength of each column of the TCOs.

DOI: 10.54254/2755-2721/7/20230545

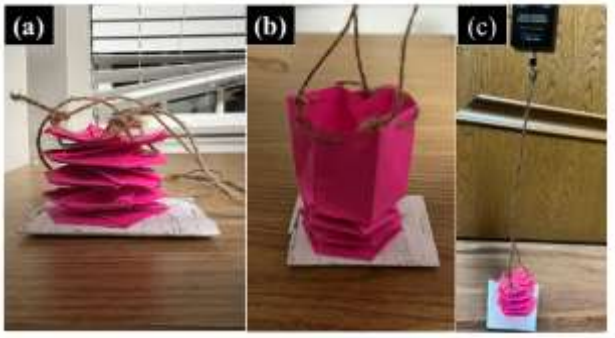

Figure 7. Photographs of a TCO (a) fixed on a horizontal surface, (b) with an upper unfolded first column, and (c) with pulling force exerted on the upper first column and the sensor measuring the force change.

4. Results and Discussion

4.1. Strain performance evaluation

In this experiment, the unfolding behaviors of the TCOs are inspected. As increasingly strong pull force is exerted on a cylinder upward with the cylinder's bottom fixed on the horizontal surface, each column is unfolded in sequence from upper ones to lower. Strains for fabricated TCO structures are calculated and plotted as a function of the number of unfolded columns in figure 8 (a). The zero columns unfolded mean that the TCO is completely folded, and the strain is zero. Two (three) columns unfolded refers to unfolding cumulatively two (three) columns after the instance of unfolding one column. Since the fourth column (the bottom column) is glued to the horizontal surface and cannot be fully unfolded, the strain data for cumulatively four columns unfolded is not used in this analysis.

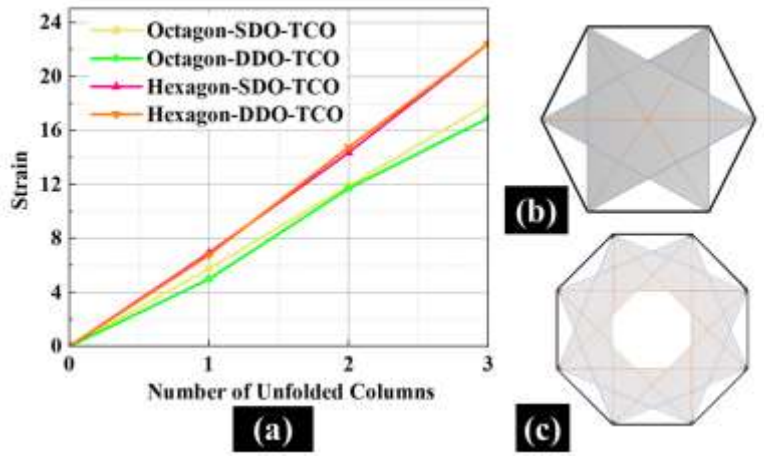

Figure 8. (a) Strain of fabricated TCO structures as a function of the number of unfolded columns. Top view of the top column of (b) hexagon (c) octagon TCO in a completely folded state. Orange and blue lines represent valley folds and mountain folds, respectively. The dotted lines are covered by upper layers, while the solid lines are creases that can be directly seen in the top view.

As can be deduced from figure 8(a), the relative direction of columns (SDO/DDO) has no significant impact on the strain of TCOs. The strain graphs for octagon-SDO and octagon-DDO are similar, though octagon-SDO offers slightly higher strain for n equals 1 and 3. When 2 (3) columns are unfolded, they have a strain of 11.92 (18.00) and 11.71 (16.93), respectively. In a similar fashion, the strain graphs of hexagon-SDO and hexagon-DDO greatly resemble each other. They have a strain of 14.38 (22.46) and 14.77 (22.46) when 2 (3) columns are unfolded, respectively.

However, the number of units in a column (n) significantly impacts the strain of triangulated cylinders. When all columns are unfolded, TCOs with six units in a column tend to stretch at a higher rate, having higher strain. The strain for hexagon TCOs is 1.29 times greater than that for octagon TCOs, which can be associated with the self-locking mechanism in hexagon TCOs. As shown in figure 8 (b), there is no room in the middle of the hexagon TCOs (the folded units are shaded in the top view). While TCOs rotate when unfolding, for a column of the hexagon TCOs, the behind units cannot move freely until the front one leaves its place. As the units in a column connect end to end, there is a large resistant force when unfolding. Hence, in the completely folded state, the self-locking mechanism holds columns

DOI: 10.54254/2755-2721/7/20230545

of hexagon TCOs in completely folded state tightly. However, in the completely folded state, octagon TCOs tend to stretch more naturally because they have a less overlapping ratio (more room in the middle) and do not have a self-locking mechanism (see figure 8 (c)). The overlapping ratio is the ratio of the overlapped area of one column to the area. The overlapped area is shaded and shown below in figure 8 (c). According to the function of strain, the octagon TCOs with larger L_0 (since they naturally stretch more) have less strain in the completely unfolded state. Similarly, hexagon TCOs with smaller L_0 (since they are held tight in the completely folded state due to the self-locking mechanism) have a larger strain in the completely unfolded state.

4.2. Strength performance evaluation

In this stage, the strength of the TCOs is evaluated. Every structure is tested three times, and the average data is calculated (See figure 9). In the experiments, the force continues to be exerted on the TCOs and is still increasing for a while in order to ensure the TCO is fully unfolded. Therefore, in the graphs, the magnitude of force continues to mount even after the last valley (three columns unfolded). Since in the experiment, the fourth columns, the bottom columns of all cylinders, are glued to a surface to fix them while collecting the unfolding force, they cannot be fully unfolded. Therefore, the data of the fourth column are not shown because they are not representative of the strength of the cylinders. Furthermore, a trend of dropping strength throughout the three trials for every TCOs is observed. This is because the repetitive folding and unfolding motion lower the strength of the creases by wearing them.

Since the octagon cylinders (fabrication #1 and #2) do not have the self-locking mechanism, so the first columns, which are the top columns, are naturally unfolded with the trend of restoring the previous state (the TCOs are deployed from the 2D pattern, so the previous state is the flat sheet). Therefore, the data of the first columns of both octagon TCOs and hexagon TCOs are not shown because those of Octagon TCOs are not representative of the strength of the cylinders and cannot be compared to those of hexagon TCOs appropriately.

The strength of different TCOs when different numbers of columns are unfolded is shown in figure 10. One can see that the number of units per column (n) plays a more prominent role in the strength of the cylinders than the relative direction of the columns (SDO/DDO) does. The hexagon cylinders typically have higher strength than octagon cylinders in both the unfolding of the second and third columns. For example, the strength for hexagon TCOs for three columns unfolded (average of SDO and DDO TCOs) is 9.06 times greater than that for octagon TCOs. The relative direction of the columns (SDO/DDO) seems to affect the strength of the octagon cylinders tiny but impacts the strength of the hexagon cylinders more significantly. The SDO one shows more strength for the hexagon cylinders than DDO one.

To sum up, the hexagon TCOs have higher strain and strength than the octagon ones, while there is no evident difference in strain and strength between SDO and DDO TCOs.

DOI: 10.54254/2755-2721/7/20230545

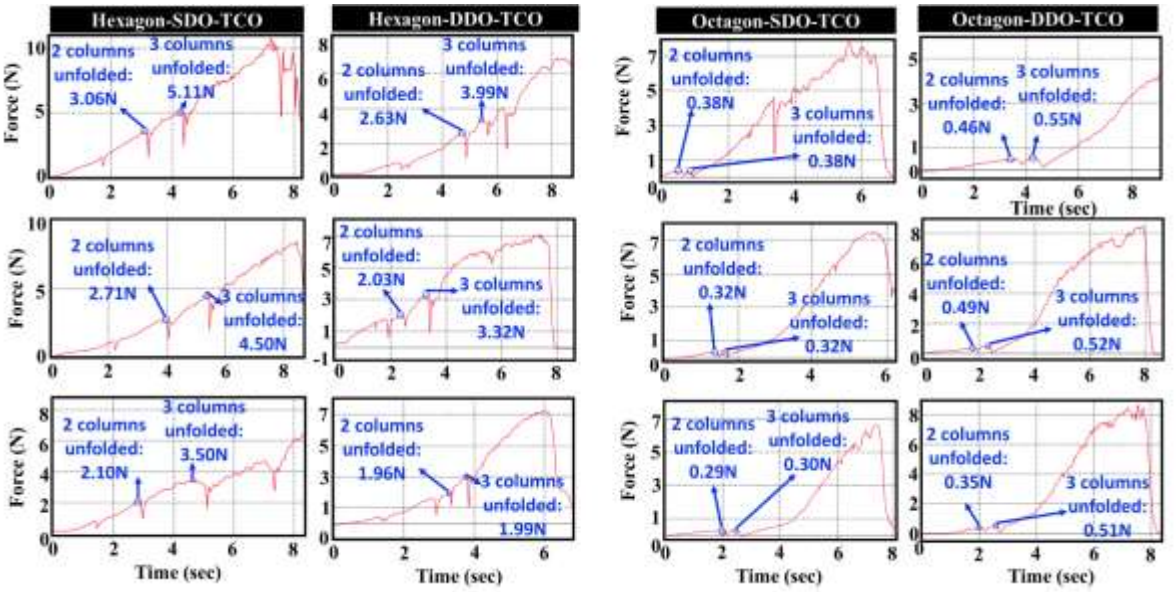

Figure 9. The force-time graphs for the hexagon and octagon TCOs. The highest strength of each trial is marked for 2 and 3 columns unfolded.

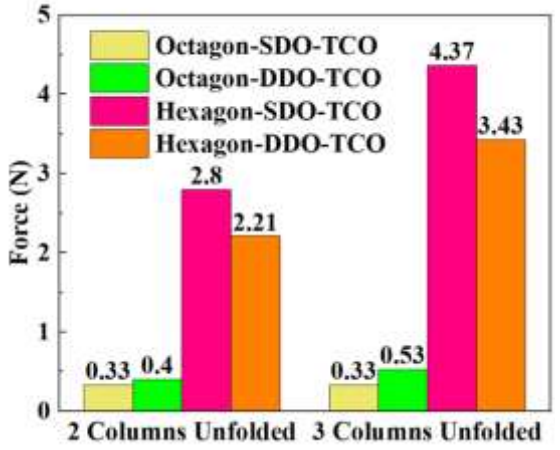

Figure 10. histogram of the strength of different TCOs when different numbers of columns are unfolded.

5. Conclusions

Origami mechanical metamaterials have attracted increasing attention thanks to their fantastic mechanical performance. With outstanding energy absorption ability, metastability, tunable stiffness, and stretchability, origami mechanical metamaterials have been applied to multiple areas, such as packed solar panels for spaceships and crash boxes for vehicles. In this paper, the effects of the number of units in each column (n) and the relative orientation of units in each column (SDO/DDO) on the strain and strength of the TCOs were experimentally investigated. It was discovered that the relative orientation of units in each column has little impact on the strain of the TCOs, while the number of units in each column plays a key role. The TCO with 6 units in each column tends to have a larger strain than the ones with 8 units. Therefore, for applications that require larger strain, which ideally stretch more after unfolding, a triangulated cylinder with 6 units in each column is recommended to reach the ideal effect compared to the ones with 8 units in each column. It was also revealed that for both TCOs with SDO and DDO units, the ones with 8 units in each column have a lower strength. The relative orientation of units in each column does not affect much the strength of the octagon-TCO, while DDO units make

hexagon-TCO stronger. Thus, for applications that require loading capacity, a hexagon TCO with DDO units is recommended to obtain the best outcome.

6. Acknowledgment

The author would like to thank Dr. Saman Farhangdoust from Stanford University, Dr. Sadegh Mehdi Aghaei from Meta Reality Labs, and Jing Li for mentoring the development of this research. The original idea of this work was inspired by the courses the authors passed in Harvard University's summer program. The science department of Darlington School provides the force sensor.

References

[1] Zhai Z, Wu L and Jiang H 2021 *Appl. Phys. Rev.* **8** 041319
[2] Tachi T 2009 *Origami* **4** 175-87
[3] Song Z, Wang X, Lv C, An Y, Liang M, Ma T, He D, Zheng Y-J, Huang S-Q and Yu H 2015 *Sci. Rep.* **5** 1-9
[4] Song Z, Ma T, Tang R, Cheng Q, Wang X, Krishnaraju D, Panat R, Chan C K, Yu H and Jiang H 2014 *Nat. Commun.* **5** 1-6
[5] Gao B, Elbaz A, He Z, Xie Z, Xu H, Liu S, Su E, Liu H and Gu Z 2018 *Adv. Mater. Technol.* **3** 1700308
[6] Bukauskas A, Koronaki A, Lee T-U, Ott D, Al Asali M W, Jalia A, Bashford T, Gatóo A, Newman J and Gattas J M 2021 *Plos one* **16** e0245737
[7] Kuribayashi K, Tsuchiya K, You Z, Tomus D, Umemoto M, Ito T and Sasaki M 2006 *Mater. Sci. Eng. A* **419** 131-7
[8] Li S, Vogt D M, Rus D and Wood R J 2017 *Proc. Natl. Acad. Sci.* **114** 13132-7
[9] Zhai Z, Wang Y, Lin K, Wu L and Jiang H 2020 *Sci. Adv.* **6** eabe2000
[10] Onal C D, Wood R J and Rus D 2012 *IEEE ASME Trans. Mechatron.* **18** 430-8
[11] Sareh P, Chermprayong P, Emmanuelli M, Nadeem H and Kovac M 2018 *Sci. Robot.* **3** eaah5228
[12] Wu S, Ze Q, Dai J, Udipi N, Paulino G H and Zhao R 2021 *Proc. Natl. Acad. Sci.* **118** e2110023118
[13] Wei Z Y, Guo Z V, Dudte L, Liang H Y and Mahadevan L 2013 *Phys. Rev. Lett.* **110** 215501
[14] Gao Y, Yi H, Li F, Tao K, Wu J, Miao J, Fu Y, Chang H and Yuan W 2021 Miura-Origami-Structured W-Tube Electret Power Generator with Water-Proof and Multifunctional Energy Harvesting Capability. In: *2021 IEEE 34th International Conference on Micro Electro Mechanical Systems (MEMS)*: IEEE) pp 728-31
[15] Liu Y, Zhang W, Zhang F, Lan X, Leng J, Liu S, Jia X, Cotton C, Sun B and Gu B 2018 *Composites Part B: Engineering* **153** 233-42
[16] Lv C, Krishnaraju D, Konjevod G, Yu H and Jiang H 2014 *Sci. Rep.* **4** 1-6
[17] Feng H, Ma J, Chen Y and You Z 2018 *Sci. Rep.* **8** 1-13
[18] Silverberg J L, Na J-H, Evans A A, Liu B, Hull T C, Santangelo C D, Lang R J, Hayward R C and Cohen I 2015 *Nat. Mater.* **14** 389-93
[19] Yasuda H, Tachi T, Lee M and Yang J 2017 *Nat. Commun.* **8** 1-7
[20] Liu K, Tachi T and Paulino G H 2019 *Nat. Commun.* **10** 1-10
[21] Xiang X, Lu G and You Z 2020 *Thin-Walled Struct.* **157** 107130
[22] Boreanaz M, Belingardi G and Maia C D F 2020 *Mater. Des. Process. Commun.* **2** e181
[23] Liu K, Tachi T and Paulino G H 2021 *J. Appl. Mech.* **88**
[24] Overvelde J T, De Jong T A, Shevchenko Y, Becerra S A, Whitesides G M, Weaver J C, Hoberman C and Bertoldi K 2016 *Nat. Commun.* **7** 1-8
[25] Zhai Z, Wang Y and Jiang H 2018 *Proc. Natl. Acad. Sci.* **115** 2032-7
[26] Mukhopadhyay T, Ma J, Feng H, Hou D, Gattas J M, Chen Y and You Z 2020 *Appl. Mater. Today* **19** 100537
[27] Wen G, Chen G, Long K, Wang X, Liu J and Xie Y M 2021 *Mater. Des.* **212** 110203

DOI: 10.54254/2755-2721/7/20230545

[28] Fang H, Chu S C A, Xia Y and Wang K W 2018 *Adv. Mater.* **30** 1706311
[29] Boatti E, Vasios N and Bertoldi K 2017 *Adv. Mater.* **29** 1700360
[30] Cai J, Estakhrianhaghighi E and Akbarzadeh A 2022 *Carbon* **191** 610-24